Biomineralization of polyanionic collagen–elastin matrices during cavarial bone repair

Lenaldo B. Rocha,[1] Randall L. Adam,[2] Neucimar J. Leite,[3] Konradin Metze,[2] Marcos A. Rossi[1]
[1]*Department of Pathology, Faculty of Medicine of Ribeirão Preto, University of São Paulo, Av. Bandeirantes, 3900, 14049-900 Ribeirão Preto, SP, Brazil*
[2]*Department of Pathology, Faculty of Medicine, UNICAMP, P.O. Box 6111, 13081-970 Campinas, SP, Brazil*
[3]*Department of Information Systems, Institute of Computing, UNICAMP, P.O. Box 6176, 13084-971 Campinas, SP, Brazil*

Received 14 September 2005; revised 18 December 2005; accepted 6 February 2006
Published online 30 June 2006 in Wiley InterScience (www.interscience.wiley.com). DOI: 10.1002/jbm.a.30782

Abstract: The polyanionic collagen–elastin matrices (PCEMs) are osteoconductive scaffolds that present high biocompatibility and efficacy in the regeneration of bone defects. In this study, the objective was to determine if these matrices are directly mineralized during the osteogenesis process and their influence in the organization of the new bone extracellular matrix. Samples of three PCEMs, differing in their charge density, were implanted into critical-sized calvarial bone defects created in rats and evaluated from 3 days up to 1 year after implantation. The implanted PCEMs were directly biomineralized by osteoblasts as shown by ultrastructural, histoenzymologic, and morphologic analysis. The removal of the implants occurred during the bone remodeling process. The organization of the new bone matrix was evaluated by image texture analysis determining the Shannon's entropy and the fractal dimension of digital images. The bone matrix complexity decreased as the osteogenesis progressed approaching the values obtained for the original bone structure. These results show that the PCEMs allow faster formation of new bone by direct biomineralization of its structure and skipping the biomaterial resorption phase. © 2006 Wiley Periodicals, Inc. J Biomed Mater Res 79A: 237–245, 2006

Key words: bone regeneration; bioabsorption; collagen; electroactive polymer; osteoconduction

INTRODUCTION

The basic design of biomaterials used for tissue regeneration aims to provide a provisional substrate for cell migration and differentiation, and new extracellular matrix deposition.[1] Of particular interest for bone regeneration therapy is the ability of a biomaterial to allow not only the deposition of new extracellular matrix but also its subsequent mineralization. Also, it is usually expected that such biomaterial should degrade in the body to provide new space for osteogenesis progression.[2,3] The presence of a biomaterial in the bone healing site should be also associated with the maintenance of the necessary extracellular signaling to keep the cellular activity.[4] Ideally, this characteristic should not be influenced by the degradation of the structure. Another important aspect of biomaterial degradation is the evidence that the biomaterial degradation rate can affect cellular survival and proliferation, and the extracellular matrix distribution and properties.[5,6]

Polyanionic collagen–elastin matrices (PCEM) are prepared by selective hydrolysis of asparagine and glutanime residues present in type I collagen α chains.[7] This process provides collagen with extra negative charges, with the possibility of controlling the number of charges added to the collagen structure according to the reaction duration.[7] The resulting material is characterized by enhanced dielectric and piezoelectric properties,[8,9] and increased number of cell adhesion motifs.[10] The hydrolysis reaction can be directly applied to a raw collagen source, like bovine pericardium or tendon, resulting in a spongy cell-free scaffold with preserved collagen and elastin microfibril structure.[7]

Biologically, the PCEMs have shown to be highly compatible with the bone healing process as demonstrated by both small[11] and critical-sized[12] bone de-

Part of this study was presented at the 22nd Annual Meeting of the Brazillian Society for Dental Research (SBPqO) in Águas de Lindóia, SP, Brazil, September 5, 2005.

Correspondence to: L.B. Rocha; e-mail: lenaldo@rpa.fmrp.usp.br

Contract grant sponsor: FAPESP; contract grant numbers: 01/05634-0, 01/08438-8, and 01/14059-0

fects models, onlay grafting experimental model,[13] and also as a membrane for periodontal furcation lesion treatment.[14] Moreover, complete recovery of bone defects can be quickly achieved with minimal inflammatory reaction.[11,12] An *in vitro* study also revealed that these matrices can also stimulate the alkaline phosphatase production by cultured osteoblasts (OSs).[15]

One aspect observed in all *in vivo* experiments was the apparent incorporation of part of the polyanionic collagen in the extracellular matrix of bone.[11–13] This could offer a unique possibility for bone regenerative therapy and tissue engineering as these scaffolds could be used as direct template for bone formation and regeneration. This study was designed to address the hypothesis that the polyanionic collagen–elastin scaffolds can be directly biomineralized *in vivo* and incorporated to the new-formed bone. We also evaluated the impact that this phenomenon could have on the remodeling process of the newly formed bone.

MATERIALS AND METHODS

Polyanionic collagen–elastin matrix preparation

Fresh bovine pericardia, originally selected for heart valve prosthesis preparation, were used as collagen source. They were treated with an alkaline solution (3 mL/g of tissue) containing 6% dimethyl sulfoxide, salts (chloride 3.0*M* and sulfate 0.9*M*) of alkaline (K^+ 1.2*M* and Na^+ 2.0*M*), and alkaline earth metal (Ca^{++} 0.91*M*) at 20°C for 24, 36, and 48 h. The resulting material was equilibrated in a solution containing salts (chloride 0.13*M* and sulfate 0.17*M*) of alkaline (K^+ 0.13*M* and Na^+ 0.7*M*) and alkaline earth metals (Ca^{++} 0.7*M*), 6 mL/g of tissue for 12 h. Excess salts were removed by rinses in 3% (w/w) boric acid solution (3 × 2 h, 250 mL), deionized water (3 × 6 h, 250 mL), followed by 0.3% (w/w) EDTA solution, pH 11 (3 × 2 h, 150 mL), and finally in deionized water (6 × 2 h, 250 mL). The matrices, now on referred as BP24, BP36, BP48, were lyophilized and kept in aseptic containers. Prior to implantation, they were cut into 4-mm discs and hydrated in sterile saline for 24 h.

Surgical procedure

Thirty-six male Wistar rats, weighting between 250 and 280 g, were obtained from our breeding colony. All procedures followed the Institutional Committee Guidelines for Laboratory Animal Use and Care.

Rats were anesthetized intramuscularly with 1 mL/kg body weight of 10% ketamine (União Química Farmacêutica SA, Embu-Guaçu, SP, Brazil) and 0.5 mL/kg body weight of 2% xylazine (Coopers Brasil, São Paulo, SP, Brazil), the skulls shaved, and the skin cleaned with an iodine solution. An incision was made over the sagittal suture and dissection was carried down to the calvarium. A full-thickness defect was created in the middle of both parietal bones using a 4-mm trephine under copious saline irrigation. The cranial sutures were not included in the defects and care was taken to avoid damage to the dura mater. After positioning one of the matrices disc within the bone defect, the periosteum was passively repositioned and the skin was sutured with 3-0 silk.

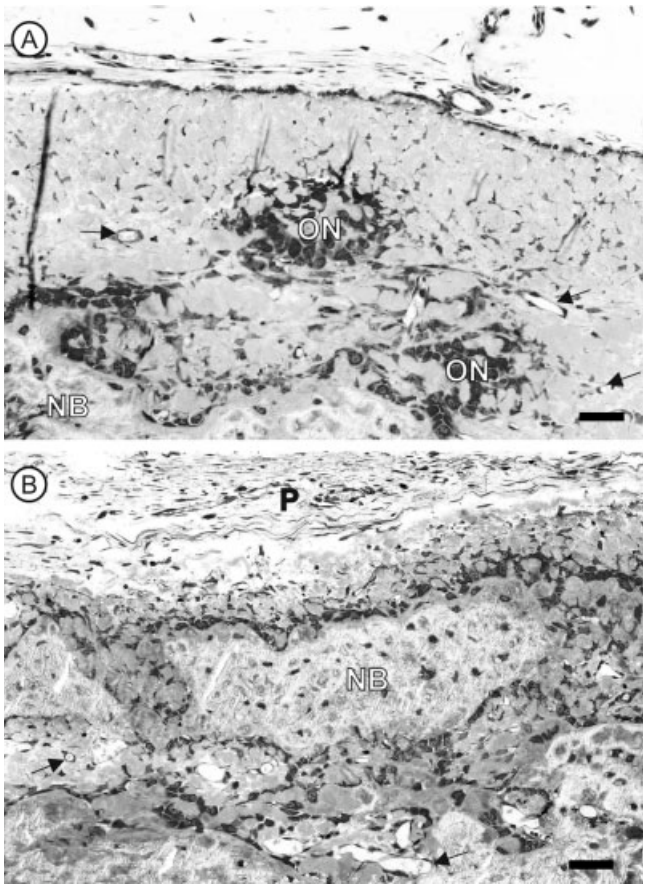

Figure 1. Morphological aspect of the osteogenesis process within the BP36 matrix 15 days after implantation showing areas of OSs nests (ON) and new formed bone (NB). Rich vascular network (arrows). There are no macrophages surrounding the ON or the NB. The periosteum (P) is populated mainly by fibroblasts. Plastic-embedded and toluidine blue-stained sections. Bar = 25 μm.

Histological processing

After 3, 7, 15, 30, 60, and 365 days, the parietal bones were resected with the surrounding soft tissues (periosteum, dura mater, and muscles) to avoid displacement of the implants. The samples were fixed with PLP[16] (2% paraformaldehyde, 0.075*M* lysine, and 0.01*M* sodium metaperiodate) prepared in 0.1*M* phosphate buffer pH 7.4 for 24 h at room temperature. Decalcification was performed with EDTA-G[17] for ~15 days. Following this, the samples were routinely processed for paraffin embedding in low-melting point paraffin (Paraplast X-Tra, Tyco Healthcare Group, Mansfied, MA). Tissue sections 5-μm thin were

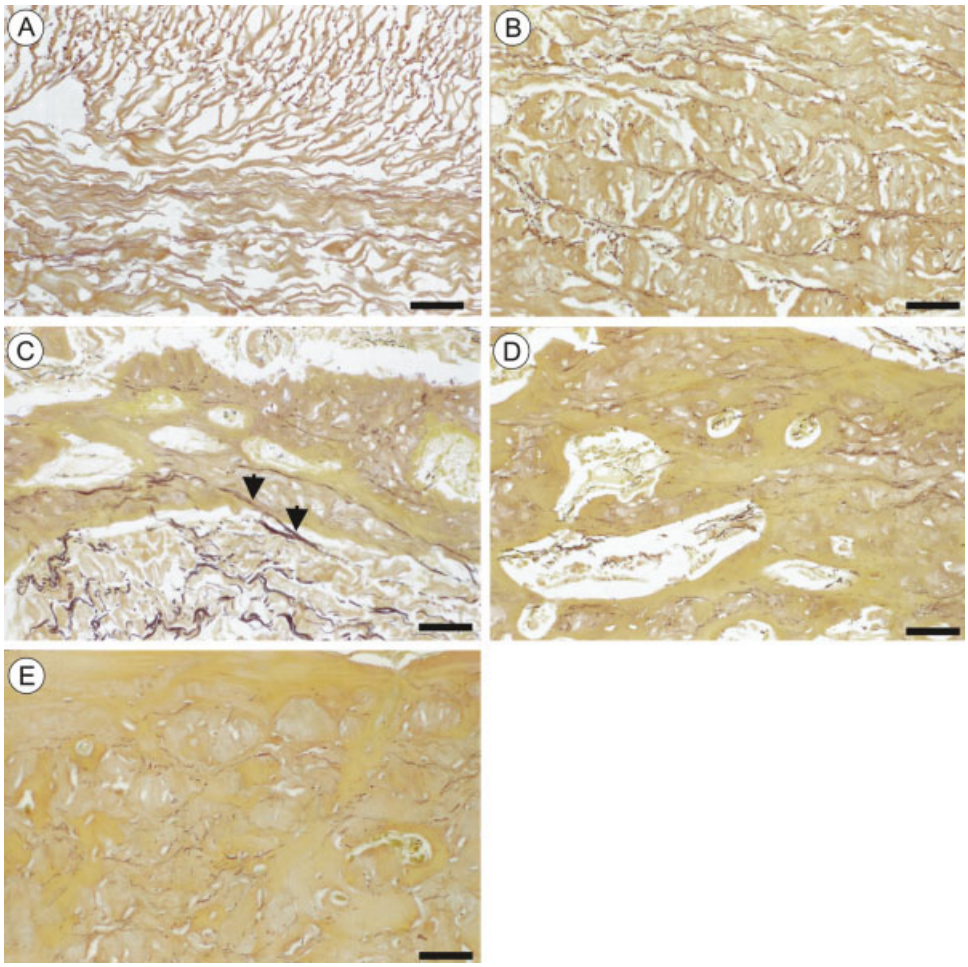

Figure 2. Weigert's resorcin/fuchsin stain for EFs of the parietals bones retrieved 3 (A), 15 (B), 30 (C), 60 (D), and 365 (E) days after implantation of the BP36 matrix. Elastic are stained in brown against a sand background. The presence of the EFs can be seen up to 1 year after the BP36 matrix implantation (day 365). In (C) it is possible to see a EF emerging from the bone extracellular matrix and continuing into the remnants of the implanted matrix. Bar = 25 μm.

stained with hematoxylin and eosin or Weigert's resorcin/fuchsin stain for elastic fibers (EFs).

Undecalcified samples were processed for resin embedding. After dehydration in ethanol, they were infiltrated and embedded in Historesin Plus (Leica Instruments AG, Heidelberg, Germany). One and a half micrometer sections were obtained using glass knife mounted microtome and stained with toluidine blue. All histological sections were analyzed and photographed with a Leica DMR microscope (Leica Microsystems AG, Wetzlar, Germany).

Phosphatases histoenzymology

For alkaline phosphatase, we used a protocol for detection in decalcified bone[18] with minor modifications. Tissue sections were deparaffinized and incubated overnight in 1% magnesium chloride in 0.1*M* Tris-maleate buffer pH 8.5. Then they were incubated for 2 h at room temperature in the enzyme substrate solution (naphtol AS-MX phosphate, 5 mg; *n*,*n*-dimethyl-formamide, 0.25 mL; fast blue BB salt, 30 mg; distilled water, 25 mL; Tris-maleate buffer pH 8.5, 25 mL; and two drops of 10% magnesium sulfate). Later, the sections were washed for 15 min in running water, counter-stained with safranin-O, and washed again. The slides were allowed to dry at room temperature for 24 h and mounted with Kaiser's glycerol jelly.

Tartarate-resistant acid phosphatase (TRAP) detection followed the above protocol with the following modifications: Tris-maleate buffer had its pH adjusted to 5, fast red ITR was used instead of fast blue BB, and the enzyme substrate also contained 0.1*M* sodium tartarate.

Immunohistochemistry

Macrophages were detected using ED-1 antibody (Serotec, Oxford, UK) by the immunoperoxidase technique. Endogenous peroxidase activity was quenched by incubating the tissue sections with 3% H_2O_2 for 20 min. Tissue sections were blocked by 1% bovine serum albumin (BSA) with 0.1*M* glycine for 30 min, then incubated with the primary antibody diluted 1:100 overnight at 4°C. Following, sections were incubated with biotinylated goat anti-mouse

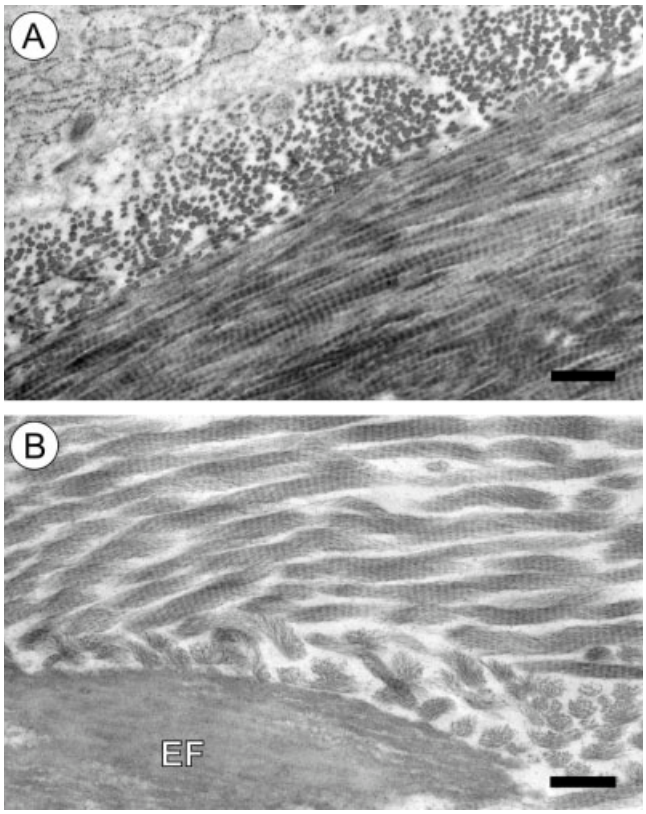

Figure 3. Ultrastructural aspect of the (A) native collagen secreted by rat OSs and (B) the polyanionic collagen of the matrix BP36. Note the difference in the fibers thickness and density and the presence of a EF in the matrix BP36. Phosphotungstic acid. Bar = 500 nm.

IgG (Vector Laboratories, Burlingame, CA) for 2 h at room temperature, and then incubated with peroxidase-conjugated avidin-biotin complex (ABC, Vector Laboratories, Burlingame, CA). Antibody complexes were visualized by addition of buffered diaminobenzidine (DAB). Sections were counterstained with Mayer's hematoxylin. The negative control slides were treated identically except that the primary antibody was omitted.

Entropy and fractal dimension analysis

For this analysis hematoxylin and eosin stained sections were used. Fifteen images from the healing site of three different animals were captured using a digital camera (Leica DC300F, Leica Microsystems AG, Heerburg, Germany). The images were captured with transmitted light with a 20× plan-fluotar objective lens, and all were captured with the same exposure time. They were saved as bitmaps without compression and using RGB color space, lately they were converted to 8-bit grayscale. Epifluorescence images were also captured as morphological reference.

The complexity of the images was measured using the entropy of information theory by Shannon[19] and the fractal dimension[20] after pseudo-3D transformation. The relationship between these data and the healing time was evaluated using mathematical regressions, comparing linear, hyperbolic, exponential, and power law models. It was chosen the method with the highest r^2. The stability of the selected model was tested using a bootstrap resampling method with substitution.

From the specimens collected 365 days after implantation, we also captured images from the nearby original bone structure. Entropy and fractal dimension of the original bone was compared with the values from the healing site using one-way analysis of variance (ANOVA) followed by Duncan's multiple comparison test.

Transmission electron microscopy

For TEM the specimens were fixed in 0.5% glutaldehyde/2% paraformaldehyde with 5% glucose in 0.1*M* cacodylate buffer pH 7.4 for 1 h. After dehydration in increasing concentrations of alcohol, the specimens were embedded in hard mixture Spurr resin (EMS, Hatfield, PA). Ultrathin sections were contrasted with phosphotungstic acid and analyzed in a Zeiss EM109 microscope (Carl Zeiss, Oberkochen, Germany) operating at 80 kV. Control samples were prepared from bone defects without implanted matrices.

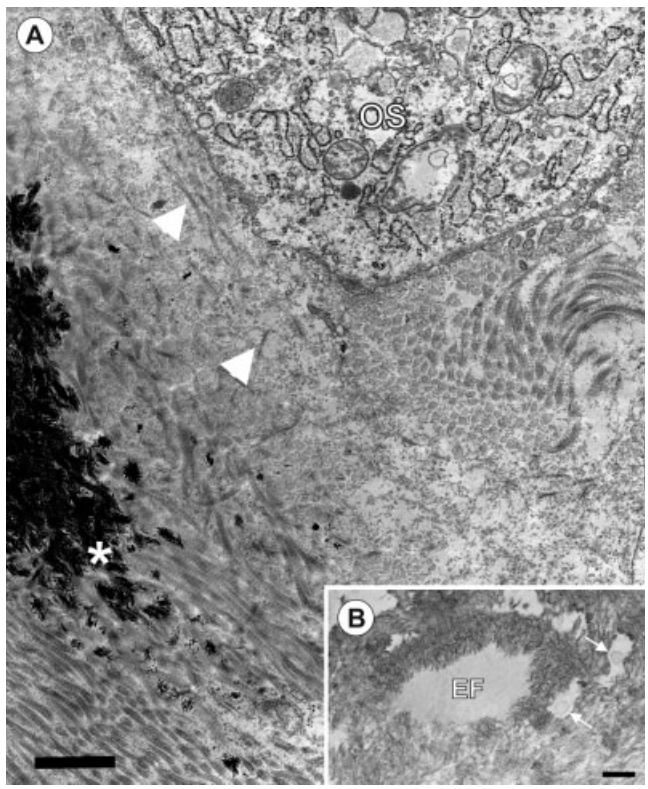

Figure 4. Ultrastructural aspect of the biomineralization (A) of the BP36 matrix (*), nearby a OS and native collagen (arrow heads) secreted by it can be seen close to the implanted matrix. (B) A EF surrounded by mineral crystals adjacent to an osteocyte extensions (arrows) is shown. Bar in A = 1 μm and bar in B = 500 nm.

RESULTS

We present here only the results for the BP36 matrix because they were the most consistent among all analysis methods. They are, however, representative of the observations made for the BP24 and BP48 matrices.

Morphological and ultrastructural analysis

Undecalcified sections of parietal bones retrieved 15 days after surgery showed areas of new formed bone in the inner portions of the BP36 matrix (Fig. 1). Clusters of OSs, mesenchymal cells, and blood vessels could be seen in the areas where the bone formation had not started yet. The structure of the mineralized matrix was contiguous to the BP36, without signs of resorption of the latter. The tissue surrounding the bone nodules was highly vascularized and rich in mesenchymal cells.

The presence of elastin was tracked at days 15, 30, 60, and 365 (Fig. 2). EFs could be found entrapped within the bone extracellular matrix at all periods, regardless the stage of maturation, from immature bone at day 15 to mature lamellar bone at day 365. However, the presence of elastin decreased as time passed.

The ultrastructural analysis of the BP36 (Fig. 3) matrix showed thicker structure than the rat bone native collagen. Also, two other aspects had changed the density of the D period that appeared lessened and presence of fibrils within the collagen fibers. The analysis of undecalcified sections retrieved 15 days after the surgery under the electron microscope showed extensive electrondense areas over the implanted matrix (Fig. 4). They were associated to the presence of OS-like cells; native collagen fibers could also be seen near the mineralizing areas. EFs were found surrounded by mineral crystals. Advanced periods had extensive periods of mineral deposits that did not allow the observation of the PCEM structure. Furthermore, the information considered relevant was that that showed the initial mineral deposition over the implanted collagen.

Histoenzimology and immunohistochemistry

Phosphatase assays and ED-1 detection was done in the samples collected 15 days after implantation (Fig. 5). Alkaline phosphatase activity was found directly over the BP36 matrix and was also related with the presence of OS-like cells. ED-1 positive cells were detected in small number and scattered within the matrix. TRAP positive cells showed morphology similar to osteoclasts and their presence was limited to bone resorption pits. Later periods were considered irrelevant as it was difficult to distinguish the bone structure from PCEM structure as previously shown,[12] nevertheless this information was not considered crucial for our analysis.

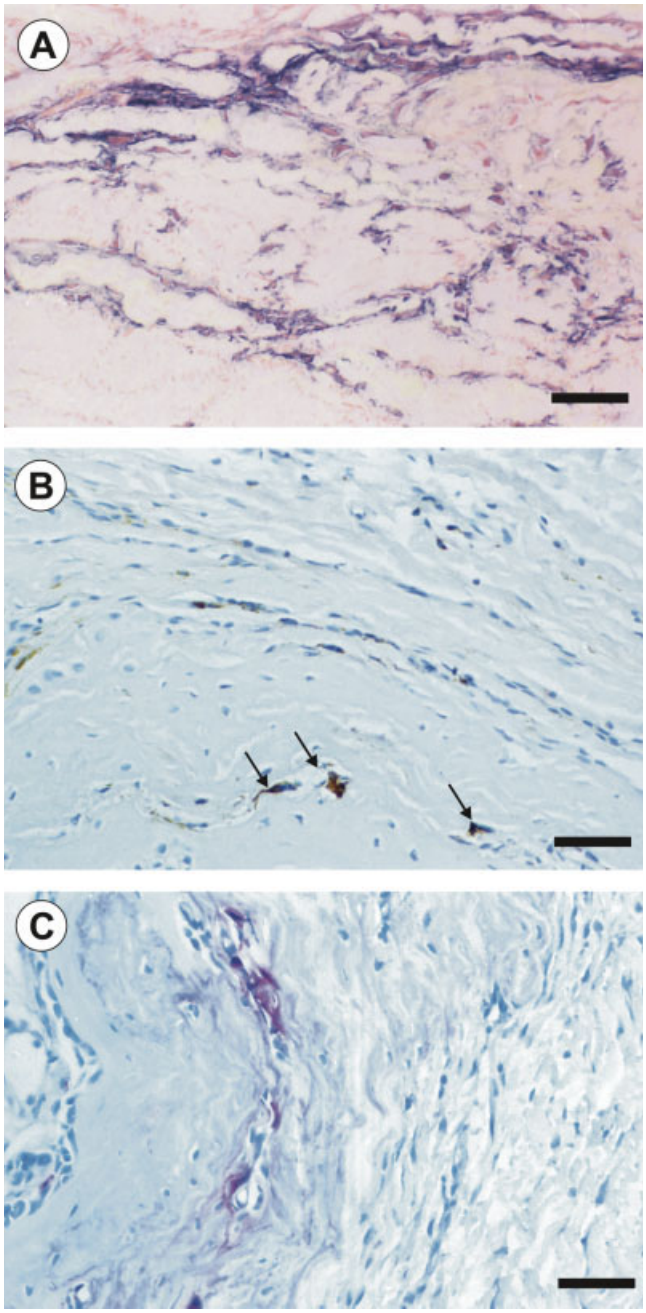

Figure 5. Photomicrographs of the alkaline phosphatase activity (A) over the structure of the BP36 matrix 15 days after implantation (blue color). After the same period only a few macrophages (arrows) could be detected by ED-1 immunohistochemistry (B). Active TRAP was found only at bone resorption pits (C), purple areas. Bar = 25 μm.

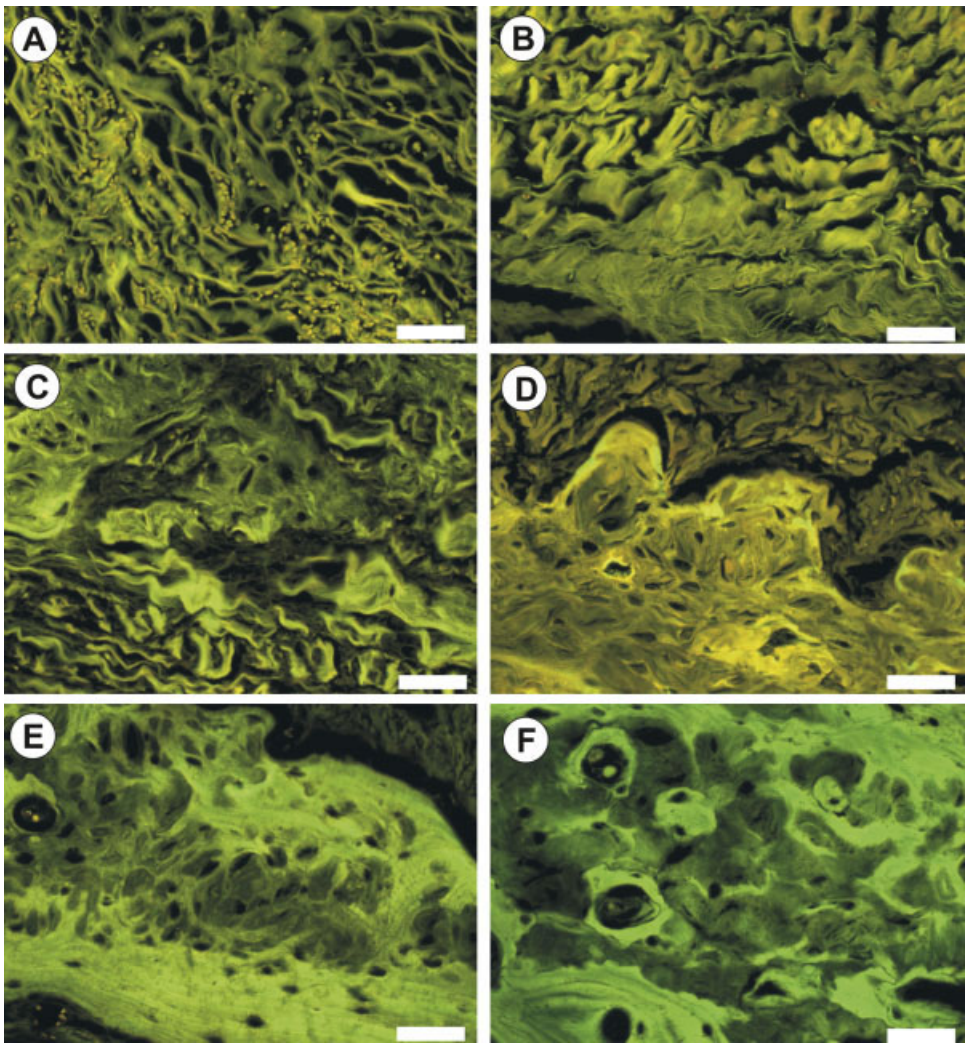

Figure 6. Organization of the extracellular matrix of the bone healing site in the presence of the BP36 matrix as revealed by epifluorescence microscopy. Despite the progressive rearrangement of the polyanionic collagen it is still possible to recognize its wavy aspect within the new formed bone. From day 60 on it is visible features of mature bone, initially lamellae and, later, osteons. Bar = 20 μm.

Bone remodeling

The observation of the hematoxylin- and eosin-stained sections with epifluorescence microscopy revealed that the organization of the BP36-implanted bone defect evolved from a sponge-like structure at days 3 and 7 after implantation to a mixture of woven bone and implanted polyanionic collagen fibers, without a clear boundary between both of them (Fig. 6). Thirty days after surgery the bone extracellular matrix was poorly organized and a few areas of BP36 matrix could still be seen. At day 60, areas of lamellar bone were clearly visible and less organized regions as well. Finally, 1 year after implantation (day 365) the new bone extracellular matrix was mixture of lamellar bone, poorly organized matrix, and secondary osteons (Fig. 7). Image texture analysis showed a quick decrease of both entropy and the fractal dimension of the healing site in the presence of the BP36 matrix. Both also showed a tendency to approach the values measured for the remaining original bone structure.

DISCUSSION

Osteoconductive biomaterials are usually expected to be removed from the bone defect during the osteogenesis process. Usually, this occurs either by solution-driven or cell mediated events that will, eventually, lead to a defect entirely filled with new formed bone only.[21] In this study, we describe the use of an osteoconductive scaffold to achieve a fully regenerated bone structure by direct *in vivo* mineralization. This process offers a distinct advantage over

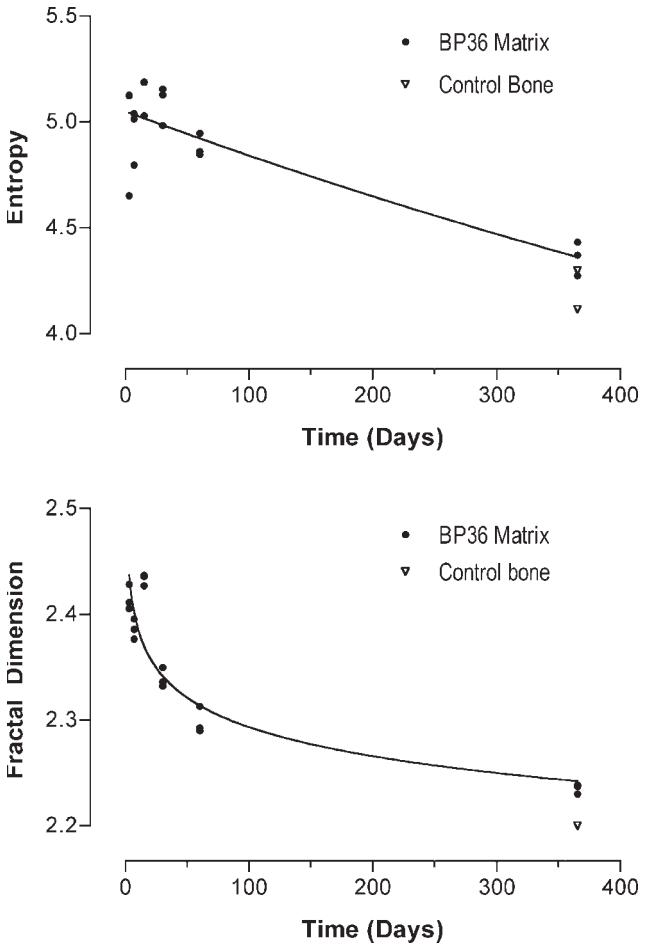

Figure 7. Hyperbolic nonlinear regression of the entropy and power-law nonlinear regression of the fractal dimension of the extracellular matrix remodeling in the bone defects that received the BP36 matrix showing the quick remodeling of the matrix. The values approached those obtained for the original bone structure 365 days after implantation. The value of r^2 for the entropy was 0.75 and for the fractal dimension was 0.81. Statistical difference was found for the fractal dimension ($p < 0.05$) but not for the entropy ($p = 0.15$) after 365 days.

the current biomaterials because the removal of the scaffolding biomaterial is no longer necessary to open space for the formation of new bone.

From the clinical point of view, this unique biological response to the PCEMs is very attractive compared to other biomaterials. Type I collagen has been proposed as scaffold for bone defects therapy.[22,23] It is commonly described as a biocompatible biomaterial that elicits low inflammatory reaction.[24–28] However, the fate of scaffolds based on this protein is largely unknown being only described as to be resorbed. Atelocollagen has been described to be incorporated into the bone structure, but this response depends on the presence of bone morphogenetic proteins associated with its structure.[29] Other biomaterials show degradation rates that is often difficult to be controlled predictively. Calcium phosphates usually degrade too slowly, often requiring macrophages and giant cells to remove its structure.[21,30] Even in fully regenerated defects it has been shown to be possible to find implant remnants entrapped within the bone structure.[31] On the other hand, some materials degrade, like polyesthers, mainly by bulk hydrolysis.[32] Despite of the design advantage changing the chemical composition of the material can control the degradation rate, debris of these materials remaining in the defect still needs to be removed by phagocytosis.

It has been previously shown that the polyanionic collagen can be mineralized *in vitro* when incubated with a saturated calcium solution.[33] This was attributed to the presence of extra carboxylic groups at the gap-overlap junction area of collagen structure that could cause the breakage of the hydrophobic barrier present in this area and that is considered to be an inhibitor of collagen mineralization.[34] *In vivo*, this characteristic of the polyanionic collagen could act as cofactor for the alkaline phosphatase secreted by the OSs facilitating the mineralization of the BP36 matrix. Moreover, the presence of the alkaline phosphatase also excluded the possibility that mineralization happened by dystrophic calcification.[35] The presence of extra negative charges in the collagen structure can create a favorable interface for ions deposition by electrostatic interaction, the same mechanism that is proposed to be responsible for the apatite layer formation in electrically polarized hydroxyapatite.[36] Also the BP36 matrix was prepared from fresh bovine pericardia, avoiding dystrophic calcification that might occur triggered by cross-linked collagen.[35,37]

The presence of elastin in the structure of the PCEM could be suspected to be nucleating the deposition of calcium salts.[38] However, because of the presence of mineral crystals only surrounding the elastin fibers, this possibility was considered unlikely. On the other hand, their presence was a useful marker of the presence of the PCEMs within the new-formed bone extracellular matrix. It was possible to detect them up to a year after implantation, revealing the long-term presence of the PCEMs, even within mature lamellar bone.

The direct biomineralization of the BP36 matrix is a positive way to accelerate the recovery of the bone defect, yet, it is highly desirable that the presence of any biomaterial within a bone defect to be transient. The presence of TRAP positive cells only at bone resorption pits strongly indicates that the BP36 removal occurs as the new-formed bone remodel. Osteoblasts could play a role in the polyanionic collagen degradation by secreting metalloproteinases, but this is a mechanism usually used for unmineralized bone matrix degradation.[39,40] The long term presence of the BP36 matrix within the bone extra-

cellular matrix did not appear to have a negative impact in the bone remodeling process as revealed by the epifluorescence and image texture analysis. The changes in the matrix reorganization from day 3 to 7 can not be attributed to any biological activity, because at these periods the BP36 implant is still poorly colonized by cells.[12] Possibly, the changes were due to fluid impregnation of the anionic collagen that is higher than native collagen.[10] From day 15 on, the whole process can be accredited to cellular activity by means of new extracellular matrix deposition and old matrix removal. As the whole process evolved features of mature bone, such as lamellae and osteons, could be seen.

The effect of the presence of the PCEM in the organization of bone was assessed determining the degree of organization of the bone matrix. The presence of lamellar bone and forming osteons gives an account of the stage of progression of bone remodeling, and could be evaluated using the entropy of information and the fractal dimension of the newformed bone. The extracellular matrix reorganized quickly as the decrease of the entropy and fractal measures revealed. The presence of hallmarks of mature bone, like lamellae and osteons, at advanced periods showed that the PCEMs had no negative impact on the turnover of the bone healing process. Moreover, the overall histological aspect of the bone formation showed that the osteogenesis process in the presence of the PCEM occurred uneventfully.

This study shows that the PCEMs might become a useful asset to surgeons dealing with bone defects and seeking for biomaterials optimized biological response to achieve faster rehabilitation of their patients. We have been working with PCEMs with three different electrical charge density and since our first study,[11] describing the biological response of them, the BP36 matrix showed the most satisfactory results; together with the observations made now, the BP36 seems to be the best PCEM for possible clinical use. Furthermore, it also seems to be a promising scaffold for *ex-vivo* bone tissue engineering.

The authors wish to thank Ms. Mônica Azevedo de Abreu, Ms. Lígia Santoro, Ms. Maria Elena Riul, and Ms. Maria Paula Montiani Scandar for their technical assistance. Drs. Marcos A. Rossi and Konradin Metze are senior investigators of the CNPq.

References

1. Putnam AJ, Mooney DJ. Tissue engineering using synthetic extracellular matrices. Nat Med 1996;2:824–826.
2. Pollok JM, Vacanti JP. Tissue engineering. Semin Pediatr Surg 1996;5:191–196.
3. Mistry AS, Mikos AG. Tissue engineering strategies for bone regeneration. Adv Biochem Eng Biotechnol 2005;94:1–22.
4. Rosso F, Marino G, Giordano A, Barbarisi M, Parmeggiani D, Barbarisi A. Smart materials as scaffolds for tissue engineering. J Cell Physiol 2005;203:465–470.
5. Bryant SJ, Anseth KS. Hydrogel properties influence ECM production by chondrocytes photoencapsulated in poly(ethylene glycol) hydrogels. J Biomed Mater Res 2002;59:63–72.
6. Alsberg E, Kong HJ, Hirano Y, Smith MK, Albeiruti A, Mooney DJ. Regulating bone formation via controlled scaffold degradation. J Dent Res 2003;82:903–908.
7. Bet MR, Goissis G, Lacerda CA. Characterization of polyanionic collagen prepared by selective hydrolysis of asparagine and glutamine carboxyamide side chains. Biomacromolecules 2001;2:1074–1079.
8. Goissis G, Piccirili L, Goes JC, de Guzzi Plepis AM, Das-Gupta DK. Anionic collagen: Polymer composites with improved dielectric and rheological properties. Artif Organs 1998; 22:203–209.
9. Góes J, Figueiró S, de Paiva J, de Vasconcelos I, Sombra A. On the piezoelectricity of anionic collagen films. J Phys Chem Solids 2002;63:465–470.
10. Bet MR, Goissis G, Vargas S, Selistre-de-Araujo HS. Cell adhesion and cytotoxicity studies over polyanionic collagen surfaces with variable negative charge and wettability. Biomaterials 2003;24:131–137.
11. Rocha LB, Goissis G, Rossi MA. Biocompatibility of anionic collagen matrix as scaffold for bone healing. Biomaterials 2002;23:449–456.
12. Rocha LB, Brochi MA, Bellucci AD, Rossi MA. Efficacy of polyanionic collagen matrices for bone defect healing. J Biomed Mater Res B Appl Biomater 2004;71:355–359.
13. Rosa FP, Lia RC, de Souza KO, Goissis G, Marcantonio E Jr. Tissue response to polyanionic collagen: Elastin matrices implanted in rat calvaria. Biomaterials 2003;24:207–212.
14. Cirelli JA, Marcantonio E Jr, Adriana R, Marcantonio C, Lia RC, Goissis G, Rossa C Jr. Evaluation of anionic collagen membranes in the treatment of class II furcation lesions: An histometric analysis in dogs. Biomaterials 1997;18:1227–1234.
15. Moreira P, An Y, Santos A Jr, Genari S. In vitro analysis of anionic collagen scaffolds for bone repair. J Biomed Mater Res B Appl Biomater 2004;71:229–237.
16. McLean I, Nakane P. Periodate–lysine–paraformaldehyde fixative. A new fixative for immunoelectron microscopy. J Histochem Cytochem 1974;22:1077–1083.
17. Mori S, Sawai T, Techima T, Kyogoku M. A new decalcifying technique for immunohistochemical studies of calcified tissue, especially applicable for cell surface marker demonstration. J Histochem Cytochem 1988;36:111–114.
18. Miao D, Scutt A. Histochemical localization of alkaline phosphatase activity in decalcified bone and cartilage. J Histochem Cytochem 2002;50:333–340.
19. Shannon C. A mathematical theory of communication. Bell Syst Tech J 1948;27:379–423.
20. Metze K, Piaza A, Piaza A, Adam R, Leite N. Texture analysis of agnor stained nuclei in lung cancer. Cell Oncol 2005;27: 137–138.
21. Lu J, Descamps M, Dejou J, Koubi G, Hardouin P, Lemaitre J, Proust J. The biodegradation mechanism of calcium phosphate biomaterials in bone. J Biomed Mater Res B Appl Biomater 2002;63:408–412.
22. DelBalso AM, Adrian JC. Collagen gel in osseous defects. A preliminary study. Oral Surg Oral Med Oral Pathol 1976;42: 562–569.
23. Moskow BS, Gold SI, Gottsegen R. Effects of scleral collagen upon the healing of experimental osseous wounds. J Periodontol 1976;47:596–606.
24. Schlegel K, Donath K, Rupprecht S, Falk S, Zimmermann R, Felszeghy E, Wiltfang J. De novo bone formation using bovine collagen and platelet-rich plasma. Biomaterials 2004;25:5387–5393.

25. Fuerst G, Gruber R, Tangl S, Mittbock M, Sanroman F, Watzek G. Effect of platelet-released growth factors and collagen type I on osseous regeneration of mandibular defects. A pilot study in minipigs. J Clin Periodontol 2004;31:784–790.
26. Gungormus M, Kaya O. Evaluation of the effect of heterelogous type I collagen on healing of bone defects. J Oral Maxillofac Surg 2002;60:541–545.
27. Lindsey W, Ogle R, Morgan R, Cantrell R, Sweeney T. Nasal reconstruction using an osteoconductive collagen gel matrix. Arch Otolaryngol Head Neck Surg 1996;122:37–40.
28. Toung J, Ogle R, Morgan R, Lindsey W. Repair of a rodent nasal critical-sized osseuos defect with osteoblast augmented collagen gel. Laryngoscope 1999;109:1580–1584.
29. Nakagawa T, Tagawa T. Ultrastructural study of direct bone formation induced by BMPs-collagen complex implanted into an ectopic site. Oral Dis 2000;6:172–179.
30. Kamakura S, Sasano Y, Shimizu T, Suzuki O, Kagayama M, Motegi K. Implanted octacalcium phosphate is more resorbable than β-tricalcium phosphate and hydroxyapatite. J Biomed Mater Res 2002;59:29–34.
31. Sarkar M, Watcher N, Patka P, Kinzl L. First histological observations on the incorporation of a novel calcium phosphate bone substitute material in the human cancellous bone. J Biomed Mater Res 2001;58:329–334.
32. Middleton J, Tipton A. Synthetic biodegradable polymers as orthopaedic devices. Biomaterials 2000;21:2335–2346.
33. Goissis G, da Silva Maginador SV, da Conceicao Amaro Martins V. Biomimetic mineralization of charged collagen matrices: In vitro and in vivo study. Artif Organs 2003;27:437–443.
34. Chapman J, Tzaphlidou M, Meek K, Kadler K. The collagen fibril—A model system for studying the staining and fixation of a protein. Electron Microsc Rev 1990;3:143–182.
35. Nimni ME, Bernick S, Cheung DT, Ertl DC, Nishimoto SK, Paule WJ, Salka C, Strates BS. Biochemical differences between dystrophic calcification of cross-linked collagen implants and mineralization during bone induction. Calcif Tissue Int 1988;42:313–320.
36. Ohgaki M, Kizuki T, Katsura M, Yamashita K. Manipulation of selective cell adhesion and growth by surface charges of electrically polarized hydroxyapatite. J Biomed Mater Res 2001; 57:366–373.
37. Vardaxis N, Boon M, Ruijgrok J. Calcification of cross-linked collagen elastin membrane implants in vivo and their proposed use in bone regeneration. Biomaterials 1996;17:1489–1497.
38. Daamen W, Nillesen S, Hafmans T, Veerkamp J, van Luyn M, van Kuppevelt T. Tissue response of defined collagen–elastin scaffolds in young and adult rats with special attention to calcification. Biomaterials 2005;26:81–92.
39. Meikle M, Bord S, Hembry R, Compston J, Croucher P, Reynolds J. Human osteoblasts in culture synthesize collagenase and other matrix metalloproteinases in response to osteotropic hormones and cytokines. J Cell Sci 1992;103:1093–1099.
40. Hill P, Orth M. Bone remodelling. Br J Orthod 1998;25:101–107.